changes in interplanar spacings calculated with vibrational effects taken into account) increase rapidly with temperature; equivalently, one can say that thermal expansion is greater near the surface than in the bulk. Second, anharmonicity already causes a substantial increase in the surface mean-square amplitudes at about half the melting temperature.

Since both of these effects should be observable by means of LEED, it would be interesting if LEED experiments (on metals or other monatomic materials) could be carried out over a wide range of temperatures to determine the importance of anharmonicity and the dependence of the mean atomic displacements upon temperature.

The method of molecular dynamics used here has two important advantages for surface calculations at temperatures above the Debye temperature, in that both anharmonic effects and mean displacements are

taken into account completely. Below the Debye temperature zero-point vibrations become important, and the classical approximation consequently breaks down. But the method described in I is most applicable at low temperatures, since this method involves the quasiharmonic approximation and the approximation of using the static, rather than dynamic, displacements. In this sense, therefore, molecular dynamics and lattice dynamics are complementary methods of investigation. Both methods have considerable potential for theoretical studies of the structure and dynamics of crystal surfaces.

ACKNOWLEDGMENT

Dielectric Function of a Model Insulator†

J. L. FRY

Department of Physics and Astronomy, Louisiana State University, Baton Rouge, Louisiana 70803

(Received 14 November 1968)

A wave-number- and frequency-dependent dielectric function has been calculated for a model insulator using the random-phase approximation. The model insulator consists of a free-electron conduction band represented by a single orthogonalized plane wave (OPW) and a valence band represented by linear combinations of ionic wave functions. All energy bands are assumed parabolic and isotropic. Numerical results are obtained for Ar, KCl, CsCl, MnS, and Si, in reasonable agreement with previous calculations. Screened exchange potentials have been obtained by using an interpolation formula, and evaluated for the chlorine ion in CsCl.

I. INTRODUCTION

THE dielectric formulation[1,2] of the many-body problem has been found especially attractive in solid-state physics, since it uses mathematical and physical concepts known to most solid-state physicists, and interprets solid-state systems in terms of familiar quantities which are accessible through experiment. Aside from its use in various schemes for calculating correlation contributions to ground-state energies,[3] the dielectric formulation has been used to understand energy loss by fast electrons in solids,[4] plasma energies,[5] and optical properties[6-8] of solids. In addition, the

dielectric formalism has been used extensively to study properties of the electron gas,[1] and quasiparticle[9] and collective[10] excitations of an electron gas containing a single point-charge impurity. Recent calculations have considered more carefully effects of the Pauli exclusion principle.[11,12] The formalism has also been used in band theory to develop a theory of self-consistent screened pseudopotentials for semiconductors[13] and more recently to develop a theory of the covalent bond in crystals.[14]

Application of the theory centers around calculation of the dielectric constant tensor $\epsilon(q,\omega)$ as a function of frequency and wave vector for the many-body system under consideration. Longitudinal or transverse components of $\epsilon(q,\omega)$ have been calculated in various approx-

* Work supported by the U. S. Air Force Office of Scientific Research.

[1] P. Nozières and D. Pines, Nuovo Cimento **9**, 470 (1958); Phys. Rev. **109**, 741 (1958); **109**, 762 (1958); **109**, 1062 (1958).

[2] D. Pines and P. Nozières, *The Theory of Quantum Liquids* (W. A. Benjamin, Inc., New York, 1966), Vol. I.

[3] P. Nozières and D. Pines, Phys. Rev. **111**, 442 (1958).

[4] R. A. Ferrell, Phys. Rev. **101**, 554 (1956).

[5] D. Pines, *Elementary Excitations in Solids* (W. A. Benjamin, Inc., New York, 1963).

[6] D. Brust, Phys. Rev. **134**, A1337 (1964).

[7] F. M. Mueller and J. C. Phillips, Phys. Rev. **157**, 600 (1967).

[8] K. S. Viswanathan and J. Callaway, Phys. Rev. **143**, 564 (1966).

[9] A. J. Layzer, Phys. Rev. **129**, 897 (1963); **129**, 908 (1963).

[10] E. A. Sziklas, Phys. Rev. **138**, A1070 (1965).

[11] D. N. Tripathy, Phys. Rev. **164**, 582 (1968).

[12] L. Kleinman, Phys. Rev. **160**, 585 (1967).

[13] M. H. Cohen and J. C. Phillips, Phys. Rev. **124**, 1818 (1961).

[14] J. C. Phillips, Phys. Rev. **166**, 832 (1968).

imations for the uniform electron gas,[15] uniform electron gas with a point impurity charge,[9,11] superconducting electron gas,[16] an isotropic model semiconductor,[17] a model insulator,[18] and a few real solids.[6,7,19,20]

An exact expression for the dielectric response function of an electron system exists, but it relies upon knowledge of exact many-electron wave functions. On the other hand, useful approximate expressions have been developed requiring knowledge of only single-electron wave functions.

The purpose of this paper is to report a random-phase-approximation (RPA) calculation of the wave number and frequency dependence of the complex longitudinal dielectric constant for a model insulator. The model used is different from the one used by Hermanson in calculating exciton levels of argon,[18] but similar in some respects to the model semiconductor of Penn.[17] The model insulator is discussed in Sec. II.

The RPA for the longitudinal dielectric function of a solid is given by[21]

$$\epsilon(\mathbf{q},\omega) = 1 - \frac{4\pi e^2}{Vq^2} \sum_{\mathbf{k}ll'} \frac{|\langle \mathbf{k}l | e^{-i\mathbf{q}\cdot\mathbf{r}} | \mathbf{k}+\mathbf{q}, l'\rangle|^2 (n_{\mathbf{k}+\mathbf{q}l'} - n_{\mathbf{k}l})}{E_{\mathbf{k}+\mathbf{q},l'} - E_{\mathbf{k},l} - (\omega + i\delta)},$$

(1)

where l' is the band index for Bloch state with momentum $\mathbf{k}+\mathbf{q}$, energy $E_{\mathbf{k}+\mathbf{q},l'}$, and occupation number $n_{\mathbf{k}+\mathbf{q},l'}$, and similarly for l. The quantity δ is an infinitesimal positive real number, arising from adiabatic boundary conditions used to derive (1), which specifies how to handle singularities of the denominator. V is the volume of the crystal. This differs from the corresponding expression for the uniform gas in two respects: the presence of Bloch matrix elements in the numerator, and occurance of energy bands in the denominator, as indicated by the band indices l, l'.

The reduced zone scheme is used, in which all wave vectors are referred to equivalent vectors in the first zone. The sum on $\mathbf{k}$ is over all vectors of the first zone, and the vector $\mathbf{k}+\mathbf{q}$ must be reduced by a vector of the reciprocal lattice if it falls outside the first zone. In this paper, terms of this type in the sum are referred to as umklapp contributions.

At zero temperature the occupation numbers $n_{\mathbf{k},l}$ are zero for conduction states and 1 for valence and core states. In what follows, only frequencies small compared to typical core-conduction–band transition frequencies will be considered; in this region of frequencies the contributions to $\epsilon(\mathbf{q},\omega)$ involving core states will be constant, so that attention will be focused only upon valence contributions to (1).
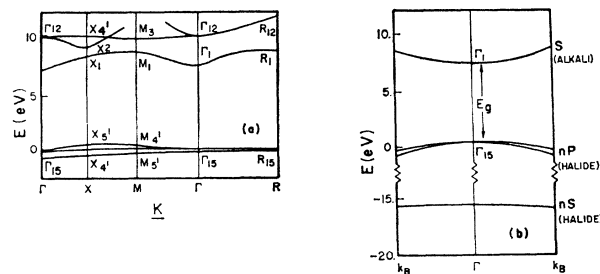

FIG. 1. (a) Energy bands of CsBr inferred by Phillips (Ref. 28), and (b) approximate energy bands used in this model. K_B is the radius of the spherical zone.

II. MODEL INSULATOR

It has been noticed[17–19] that $\epsilon(\mathbf{q},\omega)$ is not especially sensitive to the particular form of matrix elements used to evaluate Eq. (1). In addition, since behavior of all electrons in a band determine $\epsilon(\mathbf{q},\omega)$, one might hope that some simple model such as the one used by Penn[17] could be successful in predicting the general structure. However, the model used by Penn for semiconductors contains an unphysical density of states at the Fermi energy, and, in addition, the wave functions are plane-wave–like throughout most of the Brillouin zone. Thus, another model is sought for insulators which has a more physical density of states and has wave functions for electrons in the valence band more appropriate to an insulator.

Real solids which motivate this study are alkali halides and solid rare gases. Few complete band-structure calculations have been performed for these solids; some of the better calculations in this group are for KCl,[22,23] KI,[24] Ar,[25,26] and CsI.[27] Phillips has deduced band structures for a number of these insulators from optical data, and, roughly speaking, they are typified by narrow valence bands and broad conduction bands separated by energy gaps of 6 to 10 eV. The top valence bands are derived from np states of the halide ions, while the lowest conduction bands are composed mainly of ns states of the alkali ions. The halide ns bands usually lie several volts lower than the np bands. Valence band widths as a rule are much less than the minimum gap. This situation is illustrated in Fig. 1(a), which is the band structure of CsBr deduced by Phillips.[28] Although recent calculations[24,27] indicate that d bands may lie lower in the conduction bands of the alkali halides than was presumed by Phillips, this considerable complication will not be included here. With the other features in mind, however, the following model insulator is

[15] J. Lindhard, Kgl. Danske Videnskab. Selskab, Mat. Fys. Medd. **28**, 8 (1954).
[16] R. E. Prange, Phys. Rev. **129**, 2495 (1962).
[17] D. R. Penn, Phys. Rev. **128**, 2093 (1962).
[18] J. Hermanson, Phys. Rev. **150**, 660 (1966).
[19] M. Azuma, J. Phys. Soc. Japan **19**, 198 (1964).
[20] H. Nara, J. Phys. Soc. Japan **20**, 778 (1965).
[21] H. Ehrenreich and M. Cohen, Phys. Rev. **115**, 786 (1959).

[22] L. P. Howland, Phys. Rev. **109**, 1927 (1958).
[23] P. D. DeCicco, Phys. Rev. **153**, 931 (1967).
[24] Y. Onodera, M. Okazaki, and T. Inui, J. Phys. Soc. Japan **21**, 2229 (1966).
[25] R. S. Knox and F. Bassani, Phys. Rev. **124**, 652 (1961).
[26] L. F. Mattheiss, Phys. Rev. **133**, A1399 (1964).
[27] Y. Onodera, J. Phys. Soc. Japan **25**, 469 (1968).
[28] J. C. Phillips, Phys. Rev. **136**, A1705 (1964); **136**, A1714 (1964); **136**, A1721 (1964); Solid State Phys. **18**, 55 (1966).

proposed:

(1) a single conduction band composed of electrons represented by single OPW's occupying a broad parabolic energy band;

(2) a valence band composed of tightly bound electrons represented by linear combinations of np_x, np_y, and np_z, and ns atomic orbitals occupying narrow energy bands;

(3) with np and ns valence bands separated from each other and from the conduction band by finite energy gaps.

A sketch of the energy bands of this model is shown in Fig. 1(b). Although a model is sought for cubic crystals, it is necessary even in this case to make simplifying approximations to energy bands and wave functions in order to keep calculations within reason for a model. Absorption spectra of alkali halides show much stronger exciton structure than do semiconductors, so that the RPA may not be as accurate in the former case as it is in the latter. However, the RPA for this model is sufficiently difficult so that no corrections to it will be considered here. The difficulties lie in the complicated three-dimensional principal-value integrals which occur. These difficulties can be overcome by making the ansatz of spherical isotropy for all the energy bands, in which case all integrals may be reduced to one-dimensional integrals without principal-value restrictions. On the other hand the p-like character of the valence bands can be retained in matrix elements with only moderate difficulty in what follows.

Wave functions for valence bands in the tight-binding

scheme are given by the Bloch sums

$$\psi_s(\mathbf{k}) = \frac{1}{\sqrt{N}} \sum_\nu e^{i\mathbf{k}\cdot\mathbf{R}_\nu} U_s(\mathbf{r}-\mathbf{R}_\nu),$$

$$\psi_{pm}(\mathbf{k}) = \frac{1}{\sqrt{N}} \sum_\nu e^{i\mathbf{k}\cdot\mathbf{R}_\nu} U_{p,m}(\mathbf{r}-\mathbf{R}_\nu), \qquad (2.1)$$

where the sum is over all N lattice vectors R_ν at which wave function U_s and $U_{p,m}$ for the s and p ionic states, respectively, are located; m is the azimuthal quantum number for the free-ion p state. The single OPW for the conduction band is obtained by orthogonalizing a plane wave to all the lower valence and core states

$$\psi_c(\mathbf{k}) = e^{i\mathbf{k}\cdot\mathbf{r}}/\sqrt{V} - \sum_{l,m} \mu_{l,m}(\mathbf{k})\psi_{lm}(\mathbf{k}), \qquad (2.2)$$

where $\psi_{l,m}(\mathbf{k})$ are Bloch functions for the valence and core states, and $\mu_{lm}(\mathbf{k})$ are the usual orthogonalization coefficients, given by

$$\mu_{lm}(\mathbf{k}) = \left(\frac{N}{V}\right)^{1/2} \int e^{i\mathbf{k}\cdot\mathbf{r}} \psi_{lm}{}^*(\mathbf{r}) dV. \qquad (2.3)$$

Taking isotropic energy bands of the form

$$E_c(\mathbf{k}) = \alpha |\mathbf{k}|^2,$$
$$E_{pm}(\mathbf{k}) = E_{pm}{}^0 - E_{pm} |\mathbf{k}|^2,$$
$$E_s(\mathbf{k}) = E_s{}^0 - E_s |\mathbf{k}|^2,$$

converting the sum on $\mathbf{k}$ to an integral over the Brillouin zone, and writing out the sums on l and l', (1) becomes

$$\epsilon(\mathbf{q},\omega) = 1 + \frac{4\pi e^2}{q^2} \frac{2}{(2\pi)^3} \left\{ \sum_{m=-1}^{1} \left[\int_{Bz} \frac{|\langle\psi_{pm}(\mathbf{k})|e^{-i\mathbf{q}\cdot\mathbf{r}}|\psi_c(\mathbf{k}+\mathbf{q})\rangle|^2 d^3k}{(\alpha+E_{pm})k^2 + 2kq\alpha\cos\theta + \alpha q^2 + E_g - (\omega+i\delta)} \right.\right.$$

$$+ \int_{Bz} \frac{|\langle\psi_c(\mathbf{k})|e^{-i\mathbf{q}\cdot\mathbf{r}}|\psi_{pm}(\mathbf{k}+\mathbf{q})\rangle|^2 d^3k}{(\alpha+E_{pm})k^2 + 2kqE_{pm}\cos\theta + E_{pm}q^2 + E_g + \omega - i\delta} \left. \right] + \int_{Bz} \frac{|\langle\psi_s(\mathbf{k})|e^{-i\mathbf{q}\cdot\mathbf{r}}|\psi_c(\mathbf{k}+\mathbf{q})\rangle|^2 d^3k}{(\alpha+E_s)k^2 + 2kq\cos\theta + \alpha q^2 + E_{gs} - (\omega+i\delta)}$$

$$+ \int_{Bz} \frac{|\langle\psi_c(\mathbf{k})|e^{-i\mathbf{q}\cdot\mathbf{r}}|\psi_s(\mathbf{k}+\mathbf{q})\rangle|^2 d^3k}{(\alpha+E_s)k^2 + 2kqE_s\cos\theta + E_s q^2 + E_{gs} + \omega - i\delta} \left. \right\}.$$

Here E_g and E_{gs} are minimum band gaps between p-valence bands $E_{pm}(\mathbf{k})$ and conduction band $E_c(\mathbf{k})$, and s-valence band $E_s(\mathbf{k})$ and conduction band $E_c(\mathbf{k})$, respectively, and θ is the angle between $\mathbf{k}$ and $\mathbf{q}$.

At this point one is faced with the necessity of finding an appropriate set of wave functions for core and valence electrons in order to evaluate matrix elements of $e^{-i\mathbf{q}\cdot\mathbf{r}}$. A straightforward but laborious way is the numerical method of Azuma.[19] However, since interest here is in a model which hopefully will give results for a class of insulators, wave functions with adjustable parameters are chosen in order to reduce the amount of labor involved in the integrations. A form is chosen which yields analytic expressions for matrix elements.

In this same spirit a further simplification of the calculation will be made. Instead of the actual Brillouin zone, a spherical zone with the same volume is employed:

$$\tfrac{4}{3}\pi k_B{}^3 = (2\pi)^3/\Omega,$$

where Ω is the volume of the Wigner-Seitz cell, and k_B is the radius of the spherical zone.

III. MATRIX ELEMENTS

In this section, matrix elements of $e^{-i\mathbf{q}\cdot\mathbf{r}}$ are worked out for arbitrary OPW and tight-binding wave functions. Parametric wave functions are introduced to evaluate the final results. Proper normalization factors are included after the matrix elements are obtained.

The result for matrix elements of $e^{-i\mathbf{q}\cdot\mathbf{r}}$ using a single OPW and a tight-binding function is

$$\langle\psi_{lm}(\mathbf{k})|e^{-i\mathbf{q}\cdot\mathbf{r}}|\psi_c(\mathbf{k}')\rangle=\frac{1}{(NV)^{1/2}}\sum_\nu\int e^{-i\mathbf{k}\cdot\mathbf{R}_\nu}U_{lm}{}^*(\mathbf{r}-\mathbf{R}_\nu)e^{-i\mathbf{q}\cdot\mathbf{r}}e^{i\mathbf{k}\cdot\mathbf{r}}dV-\sum_{l'm'}\left(\frac{N}{V}\right)^{1/2}\left[\int e^{i\mathbf{k}'\cdot\mathbf{r}}U^*{}_{l'm'}(\mathbf{r})dV\right]$$

$$\times\frac{1}{N}\sum_{\nu\nu'}\int e^{ik\cdot\mathbf{R}_\nu}U_{lm}{}^*(\mathbf{r}-\mathbf{R}_\nu)e^{-i\mathbf{q}\cdot\mathbf{r}}e^{i\mathbf{k}'\cdot\mathbf{R}_{\nu'}}U_{l'm'}(\mathbf{r}-\mathbf{R}_{\nu'})dV. \quad(3.1)$$

Retaining only one center integrals, this simplifies to

$$\langle\psi_{lm}(\mathbf{k})|e^{-i\mathbf{q}\cdot\mathbf{r}}|\psi_c(k')\rangle=\frac{8\pi^3}{\Omega}\left(\frac{N}{V}\right)^{1/2}\delta(\mathbf{k}+\mathbf{q}-\mathbf{k}')\left[\int e^{i\mathbf{k}\cdot\mathbf{r}}U_{lm}{}^*(\mathbf{r})dV\right.$$

$$\left.-\sum_{l'm'}\int e^{i(\mathbf{k}+\mathbf{q})\cdot\mathbf{r}}U^*{}_{l'm'}(\mathbf{r})dV\int e^{-i\mathbf{q}\cdot\mathbf{r}}U_{lm}{}^*(\mathbf{r})U_{l'm'}(\mathbf{r})dV\right]. \quad(3.2)$$

Introducing the notation

$$I_{lm,l'm'}(q)\equiv\int e^{-i\mathbf{q}\cdot\mathbf{r}}U_{lm}{}^*(\mathbf{r})U_{l'm'}(\mathbf{r})dV, \quad(3.3)$$

$$|\langle\psi_{lm}(\mathbf{k})|e^{-i\mathbf{q}\cdot\mathbf{r}}|\psi_c(\mathbf{k}+\mathbf{q})\rangle|^2=(8\pi^3/\Omega)^2[\mu_{lm}{}^*(\mathbf{k})\mu_{lm}(\mathbf{k})-\mu_{lm}{}^*(\mathbf{k})\sum_{l'm'}\mu_{l'm'}(\mathbf{k}+\mathbf{q})I_{lm,l'm'}(\mathbf{q})-\mu_{lm}(\mathbf{k})$$

$$\times\sum_{l'm'}\mu^*{}_{l'm'}(\mathbf{k}+\mathbf{q})I^*{}_{lm,l'm'}(\mathbf{q})+\sum_{l'm'}\sum_{l''m''}\mu^*{}_{l'm'}(\mathbf{k}+\mathbf{q})$$

$$\times\mu_{l''m''}(\mathbf{k}+\mathbf{q})I^*{}_{lm,l'm'}(\mathbf{q})I_{lm,l''m''}(\mathbf{q})]. \quad(3.4)$$

A similar calculation gives

$$|\langle\psi_c(\mathbf{k})|e^{-i\mathbf{q}\cdot\mathbf{r}}|\psi_{lm}(\mathbf{k}+\mathbf{q})\rangle|^2=(8\pi^3/\Omega)^2[\mu_{lm}{}^*(\mathbf{k}+\mathbf{q})\mu_{lm}(\mathbf{k}+\mathbf{q})-\mu_{lm}(\mathbf{k}+\mathbf{q})\sum_{l'm'}\mu^*{}_{l'm'}(\mathbf{k})I_{l'm',lm}(\mathbf{q})$$

$$-\mu_{lm}{}^*(\mathbf{k}+\mathbf{q})\sum_{l'm'}\mu_{l'm'}(\mathbf{k})I^*{}_{l'm',lm}(\mathbf{q})+\sum_{l'm'}\sum_{l''m''}\mu^*{}_{l'm'}(\mathbf{k})$$

$$\times\mu_{l''m''}(\mathbf{k})I_{l'm',lm}(\mathbf{q})I^*{}_{l''m'',lm}(\mathbf{q})]. \quad(3.5)$$

The integrals for $\mu_{lm}(\mathbf{k})$ and $I_{lm,l'm'}(\mathbf{q})$ may be simplified by using the spherical harmonic expansion of $e^{i\mathbf{k}\cdot\mathbf{r}}$ thus,

$$\mu_{l'm'}(\mathbf{k})=\left(\frac{N}{V}\right)^{1/2}\times4\pi\sum_{l=0}^\infty i^l\sum_{m=-l}^l Y_{lm}{}^*(\theta_k,\phi_k)\int_0^\infty j_l(kr)U_{l'}{}^*(r)r^2dr\int_0^\pi\int_0^{2\pi}Y_{lm}(\theta,\phi)Y_{l'm'}(\theta,\phi)\sin\theta d\theta d\phi,$$

where $U_{l'}{}^*(r)$ is the normalized radial part of the atomic orbital with angular momentum l; θ_k and ϕ_k are the zenith and azimuthal angles of the wave vector k, and $j_l(kr)$ is a spherical Bessel function of order l. Simplifying,

$$\mu_{l'm'}(\mathbf{k})=4\pi\left(\frac{N}{V}\right)^{1/2}i^{l'}Y_{l'u'}{}^*(\theta_k,\phi_k)\int_0^\infty j_{l'}(kr)U_{l'}{}^*(r)r^2dr. \quad(3.6)$$

Similarly,

$$I_{lm,l'm'}=4\pi\sum_{l''=0}^\infty(-i)^{l''}\sum_{m''=-l''}^{l''}Y^*{}_{l''m''}(\theta_q,\phi_q)\int_0^\infty j_{l''}(qr)U_l(r)U_{l'}{}^*(r)r^2dr$$

$$\times\int_0^\pi\int_0^{2\pi}Y_{l''m''}(\theta,\phi)Y_{l'm'}(\theta,\phi)Y_{lm}{}^*(\theta,\phi)\sin\theta d\theta d\phi, \quad(3.7)$$

where θ_q and ϕ_q are the zenith and azimuthal angles for wave vector $\mathbf{q}$. The various angular relationships are pictured in Fig. 2. The angular integral is given by

$$\int_0^\pi\int_0^{2\pi}Y_{l''m''}(\theta,\phi)Y_{l'm'}(\theta,\phi)Y_{lm}{}^*(\theta,\phi)\sin\theta d\theta d\phi=\left[\frac{(2l''+1)(2l'+1)}{4\pi(2l+1)}\right]^{1/2}(l''l'm''m'|lm)\times(l''l'00|l0), \quad(3.8)$$

where the last two terms are Clebsch-Gordan coefficients in the notation of Condon and Shortley.[29] Only s and

[29] E. U. Condon and G. H. Shortley, *The Theory of Atomic Spectra* (Cambridge University Press, London, 1964).

p core and valence states are considered here, so l and l' will be either zero or 1. For these states, three separate cases arise: $l=0$, $l'=0$, or $l=l'=1$. In these cases, one has

$$I_{00,l'm'}(\mathbf{q}) = (4\pi)^{1/2}(-i)^{l'}Y_{l'm'}(\theta_q,\phi_q)\int_0^\infty j_{l'}(qr)U_{l'}(r)U_0^*(r)r^2dr,$$

$$I_{lm,00}(\mathbf{q}) = (4\pi)^{1/2}(-i)^{l}Y_{lm}^*(\theta_q,\phi_q)\int_0^\infty j_l(qr)U_0(r)U_l^*(r)r^2dr,$$

$$\hspace{6cm}(3.9)$$

$$I_{1m,1m'}(\mathbf{q}) = \delta_{m'm}\int_0^\infty j_0(qr)|U_1(r)|^2r^2dr + (8\pi)^{1/2}Y^*_{2,m-m'}(\theta_q,\phi_q)(21m-m'm'|1m)\int_0^\infty j_2(qr)|U_1(r)|^2r^2dr.$$

Evaluating Cebsch-Gordan coefficients for $m=0$, ±1; $m'=0$, ±1 yields results in terms of integrals of products of radial wave functions. Due to the angular dependence in these terms, $\epsilon(\mathbf{q},\omega)$ will not be isotropic even for the isotropic energy bands of this model. In order to simplify considerations here, it was decided to evaluate $\epsilon(\mathbf{q},\omega)$ in only one direction: q vectors along the z axis of the crystal, corresponding to a longitudinal probe propagating along the (001) direction. Other directions could be done without great difficulty, but Nara's[20] calculation for silicon suggests that this is probably not a bad average over directions, if an average is desired for a screening calculation, for example.

Equations (3.4) and (3.5) include all core states, even if matrix elements are desired only between conduction and valence states. Hence, in this model of an insulator, valence and core states affect $\epsilon(\mathbf{q},\omega)$ in two different ways: directly through transitions at a frequency $\omega=E_c-E_v$ and indirectly via the OPW for the conduction states. Effects of core states are neglected

in the present calculation. This means that $\epsilon(\mathbf{q},\omega)$ will be correct only if core states lie much lower in energy than valence bands, and then only for frequencies small compared to core-conduction-band transition frequencies. Thus, in insulators like the alkali halides, only the ns and np valence bands are treated. Angular dependence of matrix elements for these valence bands may be written out by expressing all angles in terms of the angles of the vector $\mathbf{k}$, measured with respect to the z axis of the crystal in order to facilitate calculation of the sums for $\epsilon(\mathbf{q},\omega)$. The following identities are used in this case:

$$|\mathbf{k}+\mathbf{q}| \sin\theta_{\mathbf{k}+\mathbf{q},\mathbf{k}} = |\mathbf{q}| \sin\theta_\mathbf{k},$$
$$|\mathbf{k}+\mathbf{q}| \cos\theta_{\mathbf{k}+\mathbf{q},\mathbf{k}} = |\mathbf{k}| + |\mathbf{q}| \cos\theta_\mathbf{k},$$
$$|\mathbf{k}+\mathbf{q}| \sin\theta_{\mathbf{k}+\mathbf{q},\mathbf{q}} = |\mathbf{k}| \sin\theta_\mathbf{k},\hspace{2cm}(3.10)$$
$$|\mathbf{k}+\mathbf{q}| \cos\theta_{\mathbf{k}+\mathbf{q},\mathbf{q}} = |\mathbf{q}| + |\mathbf{k}| \cos\theta_\mathbf{k},$$
$$\phi_{\mathbf{k}+\mathbf{q}}=\phi_\mathbf{k}.$$

The matrix element for the p_z band, which is identified by $l=1$, $m=0$, is

$$|\langle\psi_{10}(\mathbf{k})|e^{-i\mathbf{q}\cdot\mathbf{r}}|\psi_c(\mathbf{k}+\mathbf{q})\rangle|^2$$

$$=\left(\frac{8\pi^3}{\Omega}\right)^2\frac{12\pi N}{V}\left\{\cos^2\theta\left|\int_0^\infty j_1(kr)U_1(r)r^2dr\right|^2 + 2\cos\theta\int_0^\infty j_1(kr)U_1(r)r^2dr\int_0^\infty j_0(|\mathbf{k}+\mathbf{q}|r)U_0(r)r^2dr\right.$$

$$\times\int_0^\infty j_0(qr)U_0(r)U_1(r)r^2dr + \frac{2\cos\theta(|\mathbf{q}|+|\mathbf{k}|\cos\theta)}{|\mathbf{k}+\mathbf{q}|}\int_0^\infty j_1(kr)U_1(r)r^2dr\int_0^\infty j_1(|\mathbf{k}+\mathbf{q}|)U_1(r)r^2dr$$

$$\times\left[\int_0^\infty j_0(qr)|U_1(r)|^2r^2dr - 2\int_0^\infty j_2(qr)|U_1(r)|^2r^2dr\right] + \left|\int_0^\infty j_0(|\mathbf{k}+\mathbf{q}|r)U_0(r)r^2dr\right|^2$$

$$\times\left|\int_0^\infty j_0(qr)U_0(r)U_1(r)r^2dr\right|^2 - \frac{2(|\mathbf{q}|+|\mathbf{k}|\cos\theta)}{|\mathbf{k}+\mathbf{q}|}\int_0^\infty j_0(|\mathbf{k}+\mathbf{q}|r)U_0(r)r^2dr\int_0^\infty j_1(|\mathbf{k}+\mathbf{q}|r)U_1(r)r^2dr$$

$$\times\int_0^\infty j_0(qr)U_0(r)U_1(r)r^2dr\left[\int_0^\infty j_0(qr)|U_1(r)|^2r^2dr - 2\int_0^\infty j_2(qr)|U_1(r)|^2r^2dr\right]$$

$$+\frac{(|\mathbf{q}|^2+2|\mathbf{q}||\mathbf{k}|\cos\theta+|\mathbf{k}|^2\cos^2\theta)}{|\mathbf{k}+\mathbf{q}|^2}\left|\int_0^\infty j_1(|\mathbf{k}+\mathbf{q}|r)U_1(r)r^2dr\right|^2$$

$$\times\left.\left[\int_0^\infty j_0(qr)|U_1(r)|^2r^2dr - 2\int_0^\infty j_2(qr)|U_1(r)|^2r^2dr\right]^2\right\}.\hspace{1cm}(3.11)$$

For the p_x and p_y bands, the result is simpler, since the s-valence states drop out

$$|\langle\psi_{11}(\mathbf{k})|e^{-i\mathbf{q}\cdot\mathbf{r}}|\psi_c(\mathbf{k}+\mathbf{q})\rangle|^2$$

$$=|\langle\psi_{1-1}(\mathbf{k})|e^{-i\mathbf{q}\cdot\mathbf{r}}|\psi_c(\mathbf{k}+\mathbf{q})\rangle|^2=\left(\frac{8\pi^3}{\Omega}\right)\frac{12\pi}{2}\sin^2\theta\left\{\left|\int_0^\infty j_1(kr)U_1(r)r^2dr\right|^2-\frac{2|\mathbf{k}|}{|\mathbf{k}+\mathbf{q}|}\int_0^\infty j_1(|\mathbf{k}+\mathbf{q}|r)U_1(r)r^2dr\right.$$

$$\times\int_0^\infty j_1(kr)U_1(r)r^2dr\left[\int_0^\infty j_0(qr)|U_1(r)|^2r^2dr+\int_0^\infty j_2(qr)|U_1(r)|^2r^2dr\right]+\frac{|\mathbf{k}|^2}{|\mathbf{k}+\mathbf{q}|^2}\left|\int_0^\infty j_1(|\mathbf{k}+\mathbf{q}|r)U_1(r)r^2dr\right|^2$$

$$\times\left[\int_0^\infty j_0(qr)|U_1(r)|^2r^2dr+\int_0^\infty j_2(qr)|U_1(r)|^2r^2dr\right]^2\right\}. \quad (3.12)$$

Similar expressions obtain for matrix elements

$$\langle\psi_c(\mathbf{k})|e^{-i\mathbf{q}\cdot\mathbf{r}}|\psi_{1m}(\mathbf{k}+\mathbf{q})\rangle.$$

These matrix elements are taken with wave functions which have not been normalized explicitly, so normalization must be obtained. For the valence tight-binding wave functions

$$\int\psi_{lm}^*\psi_{l'm'}d\mathbf{V}$$

$$=\frac{1}{N}\sum_{\nu\nu'}\int e^{-i\mathbf{k}\cdot\mathbf{R}_\nu}U_{lm}^*(\mathbf{r}-\mathbf{R}_\nu)e^{i\mathbf{k}\cdot\mathbf{R}_{\nu'}}U_{l'm'}(\mathbf{r}-\mathbf{R}_\nu)d\mathbf{V}$$

$$=\sum_\nu e^{i\mathbf{k}\cdot\mathbf{R}_\nu}\int U_{lm}^*(\mathbf{r})U_{l'm'}(\mathbf{r}-\mathbf{R}_\nu)d\mathbf{V}$$

$$=1+\sum_{\nu'\neq0}e^{i\mathbf{k}\cdot\mathbf{R}_{\nu'}}\int U_{lm}^*(\mathbf{r})U_{l'm'}(\mathbf{r}-\mathbf{R}_{\nu'})d\mathbf{V}. \quad (3.13)$$

Neglecting overlap integrals, the tight-binding Bloch functions are normalized if the atomic wave functions are normalized. The OPW's are normalized by the condition

$$A^2\int|\psi_{\text{OPW}}(\mathbf{k})|^2d\mathbf{V}=1,$$

which leads to

$$1/A=(1-\sum_j\mu_{kj}^*\mu_{kj})^{1/2}. \quad (3.14)$$

Orthogonality of conduction and valence-band wave functions is also important in the present calculation. If they are not orthogonal, an incorrect long-wavelength limit is found for $\epsilon(\mathbf{q},\omega)$. If the orthogonality integral is not zero, matrix elements of $e^{-i\mathbf{q}\cdot\mathbf{r}}$ approach a constant as q approaches zero, and (1) diverges like $|\mathbf{q}|^{-2}$, indicating metallic behavior. However, choice of an OPW for the conduction band assures orthogonality,

and the matrix elements approach a constant times $|\mathbf{q}|$, as $\mathbf{q}$ approaches zero, and $\epsilon(\mathbf{q},\omega)$ obtains a finite value, as it should for an insulator.

There remains only the choice of wave functions for the valence bands. Two parametric radial wave functions are chosen:

$$U_0(r)=[\tfrac{1}{2}(2\gamma)^3]^{1/2}e^{-\gamma r} \quad (3.15)$$

for the s band, and

$$U_1(r)=[(2\delta)^5/24]^{1/2}re^{-\delta r} \quad (3.16)$$

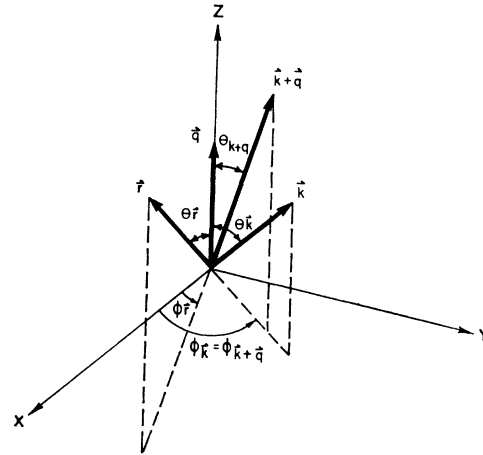for the p states. These wave functions represent the

FIG. 2. Angular relationships between $\mathbf{k}$, $\mathbf{k}+\mathbf{q}$, $\mathbf{q}$ and $\mathbf{r}$.

radial part of the atomic wave functions which compose the Bloch sums, and are properly normalized. Methods of determining the parameters δ and γ will be discussed later. With these wave functions, integrals needed for the matrix elements of $e^{-i\mathbf{q}\cdot\mathbf{r}}$ can be obtained and are tabulated in the Appendix.

Inserting these integrals in (3.11) and (3.12) gives

$$|\langle\psi_{11}(\mathbf{k})|e^{-i\mathbf{q}\cdot\mathbf{r}}|\psi_c(\mathbf{k}+\mathbf{q})\rangle|^2$$

$$=|\langle\psi_{1-1}(\mathbf{k})|e^{-i\mathbf{q}\cdot\mathbf{r}}|\psi_c(\mathbf{k}+\mathbf{q})\rangle|^2=\frac{4\pi N}{V}\left(\frac{8\pi^3}{\Omega}\right)^2\sin^2\theta\ (2\delta)^7k^2\{(\delta^2+k^2)^{-6}-2[(\delta^2+k^2+q^2+2kq\cos\theta)^3(\delta^2+k^2)^3]^{-1}$$

$$\times(2\delta)^6[(2\delta)^2+q^2]^{-3}+(\delta^2+k^2+q^2+2kq\cos\theta)^{-6}(2\delta)^{12}[(2\delta)^2+q^2]^{-6}\}, \quad (3.17)$$

$$|\langle\psi_{10}(\mathbf{k})|e^{-i\mathbf{q}\cdot\mathbf{r}}|\psi_c(\mathbf{k}+\mathbf{q})\rangle|^2$$

$$=4\pi\frac{N}{V}\left(\frac{8\pi^3}{\Omega}\right)^2\left\{\frac{2(2\delta)^7k^2\cos^2\theta}{(\delta^2+k^2)^6}+\frac{(2\delta)^6(2\delta)^4k\,\cos\theta}{(\delta^2+k^2+q^2+2kq\,\cos\theta)^2(\delta^2+k^2)^3}\frac{[3(\gamma+\delta)^2-q^2]}{[(\gamma+\delta)^2+q^2]^3}-\frac{k\,\cos\theta(q+k\,\cos\theta)}{(\delta^2+k^2+q^2+2kq\,\cos\theta)^3(\delta^2+k^2)^3}\right.$$

$$\times4(2\delta)^7(2\delta)^6\frac{[(2\delta)^2-5q^2]}{[(2\delta)^2+q^2]^4}+\frac{(2\delta)^8(2\delta)^5}{(\delta^2+k^2+q^2+2kq\,\cos\theta)^4}\frac{1}{8}\frac{[3(\gamma+\delta)^2-q^2]^2}{[(\gamma+\delta)^2+q^2]}$$

$$-\frac{(q+k\,\cos\theta)}{(\delta^2+k^2+q^2+2kq\,\cos\theta)^2(\delta^2+k^2+q^2+2kq\,\cos\theta)^3}\frac{[(2\delta)^2-5q^2]}{[(2\delta)^2+q^2]}\frac{[3(\gamma+\delta)^2-q^2]}{[(\gamma+\delta)^2+q^2]^3}$$

$$\left.+\frac{(q^2+2qk\,\cos\theta+k^2\cos^2\theta)}{(\delta^2+k^2+2kq\,\cos\theta+q^2)^6}\frac{2(2\delta)^{19}[(2\delta)-5q^2]^2}{[(2\delta)^2+q^2]^8}\right\}. \qquad (3.18)$$

In alkali halides and rare-gas solids the ns bands are well separated from np bands, so they will not be included in the numerical calculations which follow, in order that a substantial simplification of angular integrals can be made. Neglect of ns valence bands will be felt most strongly in the OPW normalization factors and in the OPW's themselves through effects of orthogonalization.

Neglecting s-band effects and normalizing, the result for the p_z band is

$$|\langle\psi_{10}(\mathbf{k}-\mathbf{q})|e^{-i\mathbf{q}\cdot\mathbf{r}}|\psi_c(\mathbf{k})\rangle|^2=4\pi\frac{N}{V}\left(\frac{8\pi^3}{\Omega}\right)^2 2(2\delta)^7\left[1-8\pi\frac{N}{V}\frac{(2\delta)^7k^2}{(\delta^2+k^2)^6}\right]^{-1}\left\{\frac{(k^2\cos^2\theta-2kq\,\cos\theta+q^2)}{(\delta^2+k^2+q^2-2kq\,\cos\theta)^6}-\frac{2[(2\delta)^2-5q^2]}{(\delta^2+k^2)^3}\right.$$

$$\left.\times\frac{(k^2\cos^2\theta-kq\,\cos\theta)(2\delta)^6}{(\delta^2+k^2+q^2-2kq\,\cos\theta)[(2\delta)^2+q^2]^4}+(2\delta)^{12}\frac{[(2\delta)^2-5q^2]^2}{[(2\delta)^2+q^2]^8}\frac{k^2\cos^2\theta}{(\delta^2+k^2)^6}\right\}, \qquad (3.19)$$

$$|\langle\psi_c(\mathbf{k})|e^{-i\mathbf{q}\cdot\mathbf{r}}|\psi_{10}(\mathbf{k}+\mathbf{q})\rangle|^2=4\pi\frac{N}{V}\left(\frac{8\pi^3}{\Omega}\right)^2 2(2\delta)^7\left[1-8\pi\frac{N}{V}\frac{(2\delta)^7k^2}{(\delta^2+k^2)^6}\right]^{-1}\left\{\frac{k^2\cos^2\theta+2kq\,\cos\theta+q^2}{(\delta^2+k^2+q^2+2kq\,\cos\theta)^6}\right.$$

$$\left.-\frac{2(2\delta)^6[(2\delta)^2-5q^2]}{(\delta^2+k^2)^3[(2\delta)^2+q^2]^4}\frac{(k^2\cos^2\theta+kq\,\cos\theta)}{(\delta^2+k^2+2kq\,\cos\theta)^3}+(2\delta)^{12}\frac{[(2\delta)^2-5q^2]^2k^2\cos^2\theta}{[(2\delta)^2+q^2]^8(\delta^2+k^2)^6}\right\}. \qquad (3.20)$$

Matrix elements needed for p_x and p_y bands are

$$|\langle\psi_{11}(\mathbf{k}-\mathbf{q})|e^{-i\mathbf{q}\cdot\mathbf{r}}|\psi_c(\mathbf{k})\rangle|^2=4\pi\frac{N}{V}\left(\frac{8\pi^3}{\Omega}\right)^2(2\delta)^7k^2\sin^2\theta\left[1-8\pi\frac{N}{V}\frac{(2\delta)^7k^2}{(\delta^2+k^2)^6}\right]^{-1}\left\{\frac{1}{(\delta^2+k^2+q^2-2kq\,\cos\theta)^6}\right.$$

$$\left.-\frac{(2\delta)^6}{[(2\delta)^2+q^2]^3}\frac{2}{(\delta^2+k^2+q^2-2kq\,\cos\theta)^3(\delta^2+k^2)^3}+\frac{1}{(\delta^2+k^2)^6}\frac{(2\delta)^{12}}{[(2\delta)^2+q^2]^6}\right\} \qquad (3.21)$$

and

$$|\langle\psi_c(\mathbf{k})|e^{-i\mathbf{q}\cdot\mathbf{r}}|\psi_{11}(\mathbf{k}+\mathbf{q})\rangle|^2=4\pi\frac{N}{V}\left(\frac{8\pi^3}{\Omega}\right)^2(2\delta)^7k^2\sin^2\theta\left[1-8\pi\frac{N}{V}\frac{(2\delta)^7k^2}{(\delta^2+k^2)^6}\right]^{-1}\left\{\frac{1}{(\delta^2+k^2+q^2+2kq\,\cos\theta)^6}\right.$$

$$\left.-\frac{(2\delta)^6}{[(2\delta)^2+q^2]^3}\frac{2}{(\delta^2+k^2+q^2+2kq\,\cos\theta)^3(\delta^2+k^2)^3}+\frac{1}{(\delta^2+k^2)^6}\frac{(2\delta)^{12}}{[(2\delta)^2+q^2]^6}\right\}. \qquad (3.22)$$

A transformation has been anticipated in (3.19) and (3.21) to remove angular dependences from the OPW normalization factors. This transformation makes it possible to do principal-value integrals over angles exactly and avoid the difficulty of numerical principal-value integrals. A corresponding transformation must be made in energy denominators when using transformed matrix elements.

IV. SUMMATIONS

Necessary ingredients for computing the RPA dielectric function have now been obtained, so there remains only the sum over states in the first Brillouin zone to be performed. This sum has been changed to an integral using the spherical-zone approximation. It is further assumed that the p_x and p_y bands are degenerate throughout the zone with reciprocal effective

mass $2E_{11}$, while the p_z band has reciprocal effective mass $2E_{10}$. No splitting of the p_z band at $k=0$ has been introduced, although it is a simple matter to do so. The small spin-orbit splittings for insulators under consideration here do not merit introduction of yet another parameter into the model.

In order to remove complicated angular dependence from the OPW normalization factors in matrix elements of the type $\langle \psi_v(\mathbf{k}) | e^{-i\mathbf{q}\cdot\mathbf{r}} | \psi_c(\mathbf{k}+\mathbf{q}) \rangle$, the following transformation is made on $\mathbf{k}$:

$$\mathbf{k}' = \mathbf{k} + \mathbf{q}. \qquad (4.1)$$

Limits of integration are then determined by the conditions

$$0 \leq |\mathbf{k}|^2 \leq k_B{}^2, \quad |\mathbf{k}'-\mathbf{q}|^2 \leq k_B{}^2,$$
$$0 \leq |\mathbf{k}'|^2 + |\mathbf{q}|^2 - 2|\mathbf{k}'||\mathbf{q}| \cos\theta \leq k_B{}^2, \qquad (4.2)$$

where $\cos\theta$ is the angle between $\mathbf{k}$ and $\mathbf{q}$. Thus

$$X_1 \equiv \frac{|\mathbf{k}'|^2 + |\mathbf{q}|^2 - k_B{}^2}{2|\mathbf{k}'||\mathbf{q}|} \leq \cos\theta \leq \frac{|\mathbf{k}'|^2 + q^2}{2|\mathbf{k}'||\mathbf{q}|} \equiv X_2,$$

but

$$-1 \leq \cos\theta \leq 1 \qquad (4.3)$$

is the requirement on $\cos\theta$, so limits on the angular integrals must be determined from simultaneous requirements (4.2) and (4.3): $\cos\theta$ must lie between ± 1, X_1, and X_2. For the case $q \leq k_B$

$$k' = k_B + q, \quad \text{for} \quad \cos\theta = 1$$
$$k' = k_B - q, \quad \text{for} \quad \cos\theta = -1. \qquad (4.4)$$

This region of integration is shown in Fig. 3(a). On the other hand, for $q \geq k_B$, the only possibility is $\cos\theta = 1$, and $k' = q + k_B$ or $k' = q - k_B$. This region of integration is shown in Fig. 3(b).
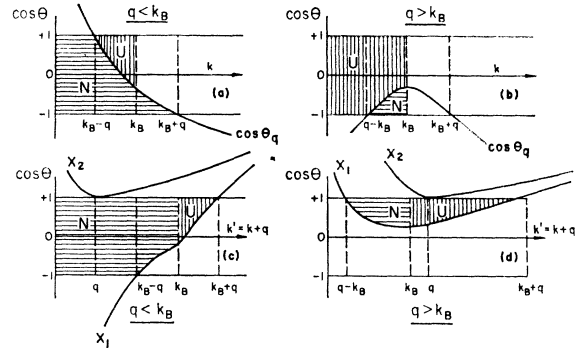

Fig. 3. Normal (N) and umklapp (U) regions of integration for different values of q.

It is interesting to determine separately the contributions to $\epsilon(\mathbf{q},\omega)$ from normal and umklapp processes. Umklapp terms arise for $|\mathbf{k}+\mathbf{q}| > k_B$, in which case it is necessary to subtract a reciprocal-lattice vector to bring $\mathbf{k}+\mathbf{q}=\mathbf{k}'$ back into the first zone. In terms of the variable $\mathbf{k}'$, normal processes occur for $|\mathbf{k}'| < k_B$, while umklapp processes come from integrals $|\mathbf{k}'| > k_B$. These regions are indicated in Figs. 3(a) and 3(b). For integrals over untransformed matrix elements, normal and umklapp contributions may be separated by defining

$$\cos\theta_q \equiv (k_B{}^2 - |\mathbf{k}|^2 - |\mathbf{q}|^2)/2|\mathbf{k}||\mathbf{q}|. \qquad (4.5)$$

Normal processes occur when $|\mathbf{k}+\mathbf{q}|^2 \leq k_B{}^2$, umklapp when $|\mathbf{k}+\mathbf{q}| \geq k_B{}^2$. Thus, the two regions of integration are

$$-1 \leq \cos\theta \leq \cos\theta_q \leq 1, \quad \text{for normal}$$
$$-1 \leq \cos\theta_q \leq \cos\theta \leq 1, \quad \text{for umklapp}.$$

This is illustrated in Figs. 3(c) and 3(d).

For the purpose of numerical calculations it is convenient to separate real and imaginary parts of $\epsilon(\mathbf{q},\omega)$. Including transformation (4.1) where needed

$$\mathrm{Re}\,\epsilon(\mathbf{q},\omega) \equiv \epsilon_1(\mathbf{q},\omega) = 1 + \frac{4\pi e^2}{q^2} \frac{2}{(2\pi)^3} \left\{ P \int_{\mathrm{Bz'}} \frac{|\langle \psi_{10}(\mathbf{k}-\mathbf{q}) | e^{-i\mathbf{q}\cdot\mathbf{r}} | \psi_c(\mathbf{k}) \rangle|^2 d^3k}{E_c(\mathbf{k}) - E_{10}(\mathbf{k}-\mathbf{q}) - \omega} + \int_{\mathrm{Bz}} \frac{|\langle \psi_c(\mathbf{k}) | e^{-i\mathbf{q}\cdot\mathbf{r}} | \psi_{10}(\mathbf{k}+\mathbf{q}) \rangle|^2 d^3k}{E_c(\mathbf{k}) - E_{10}(\mathbf{k}-\mathbf{q}) + \omega} \right.$$

$$\left. + 2P \int_{\mathrm{Bz'}} \frac{|\langle \psi_{11}(\mathbf{k}-\mathbf{q}) | e^{-i\mathbf{q}\cdot\mathbf{r}} | \psi_c(\mathbf{k}) \rangle|^2 d^3k}{E_c(\mathbf{k}) - E_{11}(\mathbf{k}-\mathbf{q}) - \omega} + 2 \int_{\mathrm{Bz}} \frac{|\langle \psi_c(\mathbf{k}) | e^{-i\mathbf{q}\cdot\mathbf{r}} | \psi_{11}(\mathbf{k}+\mathbf{q}) \rangle|^2 d^3k}{E_c(\mathbf{k}) - E_{11}(\mathbf{k}+\mathbf{q}) + \omega} \right\} \qquad (4.6)$$

and

$$\mathrm{Im}\,\epsilon(\mathbf{q},\omega) \equiv \epsilon_2(\mathbf{q},\omega) = \frac{8\pi^2 e^2}{(2\pi)^3 q^2} \left\{ \int_{\mathrm{Bz'}} |\langle \psi_{10}(\mathbf{k}-\mathbf{q}) | e^{-i\mathbf{q}\cdot\mathbf{r}} | \psi_c(\mathbf{k}) \rangle|^2 \delta[E_c(\mathbf{k}) - E_{10}(\mathbf{k}-\mathbf{q}) - \omega] d^3k \right.$$

$$\left. + 2 \int_{\mathrm{Bz}} |\langle \psi_{11}(\mathbf{k}-\mathbf{q}) | e^{-i\mathbf{q}\cdot\mathbf{r}} | \psi_c(\mathbf{k}) \rangle|^2 \delta[E_c(\mathbf{k}) - E_{11}(\mathbf{k}-\mathbf{q}) - \omega] d^3k \right\}, \qquad (4.7)$$

where P indicates principal value of the integral is to be taken.

V. LONG-WAVELENGTH LIMITS

Expanding matrix elements in powers of q, the long-wavelength limits may be evaluated. The limits of interest are

$$\lim_{q \to 0} \frac{1}{q^2} |\langle \psi_{11}(\mathbf{k}-\mathbf{q}) | e^{-i\mathbf{q}\cdot\mathbf{r}} | \psi_c(\mathbf{k}) \rangle|^2 = \frac{36k^4 \cos^2\theta \sin^2\theta}{(\delta^2 + k^2)^8}, \qquad (5.1)$$

and

$$\lim_{q\to 0}\frac{1}{q^2}|\langle\psi_{10}(\mathbf{k}-\mathbf{q})|e^{-i\mathbf{q}\cdot\mathbf{r}}|\psi_c(\mathbf{k})\rangle|^2=\frac{1}{(\delta^2+k^2)^6}\left[1-\frac{6k^2\cos^2\theta}{(\delta^2+k^2)}\right]^2.\tag{5.2}$$

Inserting (5.1) and (5.2) into (4.6) and separating the different band contributions,

$$\epsilon_1^x(0,\omega)+\epsilon_1^y(0,\omega)=AP\int_0^1\frac{48}{5}\frac{X^6dX}{(\Delta^2+X^2)^8}\left[\frac{1}{(\Delta_c+\Delta_x)X^2+1-W}+\frac{1}{(\Delta_c+\Delta_x)X^2+1+W}\right],\tag{5.3}$$

$$\epsilon_1^z(0,\omega)=AP\int_0^1\frac{2X^2dX}{(\Delta^2+X^2)^6}\left[1-\frac{4X^2}{(\Delta^2+X^2)}+\frac{36}{5}\frac{X^4}{(\Delta^2+X^2)}\right]$$

$$\times\left[\frac{1}{(\Delta_c+\Delta^z)X^2+1-W}+\frac{1}{(\Delta_c+\Delta^z)X^2+1+W}\right],\tag{5.4}$$

where the following transformations have been made:

$$X\equiv k/k_B,\quad \Delta_c\equiv\alpha k_B{}^2/E_g,\quad \Delta_x=\Delta_y\equiv E_{11}k_B{}^2/E_g,$$
$$W\equiv\omega/E_g,\quad \Delta_z\equiv E_{10}k_B{}^2/E_g,\quad \Delta\equiv\delta/k_B.\tag{5.5}$$

Here

$$A\equiv\frac{32}{E_g}\frac{(2\pi)^6}{\Omega^3}(2\Delta)^7.$$

The physical meaning of these new parameters is clear from the defining equations: X, and Δ are momenta relative to the momentum at the Brillouin-zone boundary; Δ_c is the ratio of conduction-band width to the band gap; Δ_x, Δ_y, and Δ_z are ratios of valence-band widths to band gap; and W is the frequency measured in units of the gap frequency.

At zero frequency the principal-value restriction may be relaxed, and the integrals for the real part of the static dielectric constant are simple:

$$\epsilon_1^x(0)+\epsilon_1^y(0)=A\frac{48}{5}\int_0^1\frac{x^6dx}{(\Delta^2+x^2)^8}\frac{2}{(\Delta_x+\Delta_x)x^2+1},\tag{5.6}$$

$$\epsilon_1^z(0)=2A\int_0^1\left\{\left[1-\frac{4x^2}{(\Delta^2+x^2)^6}+\frac{36}{5}\frac{x^4}{(\Delta^2+x^2)^2}\right]2x^2dx\left/(\Delta^2+x^2)^6[(\Delta_c+\Delta_l)x^2+1]\right.\right\}.\tag{5.7}$$

Similarly evaluating integrals for $\epsilon_2(\mathbf{q},\omega)$ by using properties of the Dirac δ function,

$$\epsilon_2^z(0,\omega)=\frac{A}{(\Delta_c+\Delta_z)^{1/2}}\left\{\frac{(W-1)(\Delta_c+\Delta_z)^5}{[\Delta^2(\Delta_c+\Delta_z)+W-1]^6}\left[1-8\pi\frac{N}{V}\frac{(2\Delta)^7(W-1)(\Delta_c+\Delta_z)^5}{[\Delta^2(\Delta_c+\Delta_z)+W-1]^6}\right]^{-1}\right\}$$

$$\times\left[1-\frac{4(W-1)}{\Delta^2(\Delta_c+\Delta_z)+W-1}+\frac{36}{5}\left(\frac{W-1}{\Delta^2(\Delta_c+\Delta_z)+W-1}\right)^2\right]\eta(W-1)\eta(\Delta_c+\Delta_z+1-W)\tag{5.8}$$

and

$$\epsilon_2^x(0,\omega)+\epsilon_2^y(0,\omega)=\frac{A}{(\Delta_c+\Delta_x)^{1/2}}\frac{48}{5}\frac{(W-1)(\Delta_c+\Delta_x)^5}{[\Delta^2(\Delta_c+\Delta_x)+W-1]^8}\left[1-8\pi\frac{N}{V}\frac{(2\Delta)^7(W-1)(\Delta_c+\Delta_x)^5}{[\Delta^2(\Delta_c+\Delta_x)+W-1]^6}\right]^{-1}$$

$$\times\eta(W-1)\eta(\Delta_c+\Delta_x+1-W),\tag{5.9}$$

where

$$\eta(x)=0,\quad x<0$$
$$\eta(x)=1,\quad x\geq 0.$$

These limits are useful in helping to determine parameters of the model and in checking calculations with the more complicated expressions.

VI. NUMERICAL RESULTS

In this section parameters for the model are obtained for several insulators as well as one semiconductor. Numerical results for the dielectric function of this model are then compared with previous calculations, where available.

TABLE I. Band parameters used for calculation of $\epsilon(q,\omega)$ with this model.

| | Cell volume (a.u.) | Gap (eV) | P_x | Bandwidths (eV) | | | $\delta/k_B{}^a$ |
				P_z	Conduction	$\epsilon(0)$	
CsCl	386	7	0.60	0.60	1.5	2.70	1.637
KCl	418.3	9.40	0.70	2.00	4.10	2.13	1.609
Ar	250	13.3	0.20	0.60	2.70	1.70	1.820
Si	275	(1.0)	3.2	10.0	1.4	11.0	1.595
		(4.0)					1.575
MnS	237.5	6.2	1.0	1.0	3.0	6.8	1.613

^{a} k_B is the radius of the spherical zone.

Motivation for this model has been the alkali halides, for which a typical band structure is given in Fig. 1, along with the present model approximation to it. The final model may best be described by its parameters: Ω, k_B, α, E_{10}, E_{11}, E_g, and δ. Ω is the unit cell volume, which is related simply to the lattice constant through the crystal structure. k_B is the radius of the spherical zone, which is determined by Ω. α, E_{10}, and E_{11} are twice the reciprocal effective masses for conduction and valence energy bands, which are assumed parabolic and isotropic throughout the zone. E_g is the minimum gap, assumed to lie at $k=0$, and δ is a parameter in the valence-electron wave function which, roughly speaking, indicates the degree to which electrons are bound to individual ions. Thus, in this simplified model with seven parameters, there are six independent parameters which must be determined. Of these six parameters, five are found from experiment: α/E_g, E_{10}/E_g, E_{11}/E_g, E_g, and Ω. Ω has been calculated using lattice constants derived from x-ray analysis, while the others have been obtained from optical measurements. There remains one parameter not readily accessible to experiment, the valence wave-function parameter δ.

This parameter could be obtained by a best fit to the appropriate free-ion wave function; by a variational calculation using a pseudopotential for the free ion; by requiring that the longitudinal sum rule be satisfied
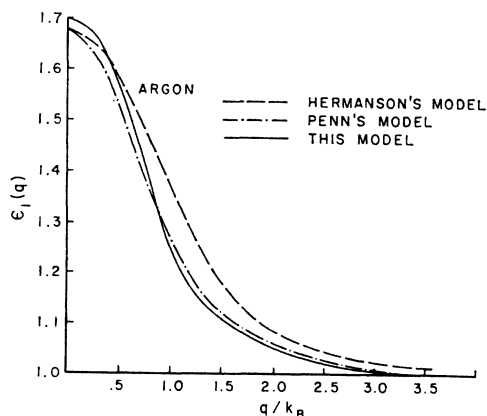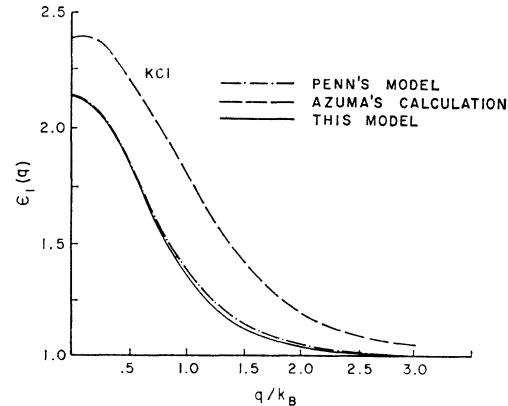

FIG. 5. Zero-frequency dielectric function for KCl.

using only the p bands and one conduction band; or by requiring that $\epsilon(q,\omega)$ obtain the measured static dielectric constant in the appropriate limits. The latter method has been chosen for these calculations.

The following insulators were examined with this model: CsCl, KCl, Ar, and MnS. In addition, the model was tested for one semiconductor, silicon. All necessary parameters were obtained from Phillips's analysis of ultraviolet absorption of insulators,[28] or from band-structure calculations.[30] Characteristic parameters for these solids are listed in Table I.

Argon, the insulator which is probably best described by this model, is discussed first. The static dielectric constant was obtained from Eqs. (5.6) and (5.7) by iterating until Δ yielded the proper result for $\epsilon(0)$. This result should be the optical dielectric constant, $n^2 = 1.70$, since the model describes only electronic contributions to $\epsilon(q,\omega)$. For the parameters listed in Table I, $\Delta = 1.82$ gave this value. Numerical calculations of $\epsilon(q)$ with the full set of parameters produced results shown in Fig. 4. Hermanson's[18] dielectric function for

TABLE II. Normal and umklapp contributions to $\epsilon(q)$ for solid argon. The total $\epsilon(q)$ is $1 + \epsilon^N(q) + \epsilon^U(q)$.

q/k_B	Normal	Umklapp	Total
0	0.700	0.0	1.700
0.05	0.690	0.009	1.699
0.10	0.675	0.020	1.695
0.15	0.656	0.031	1.688
0.20	0.635	0.041	1.677
0.25	0.610	0.051	1.661
0.30	0.584	0.062	1.644
0.35	0.555	0.071	1.625
0.40	0.524	0.080	1.602
0.45	0.490	0.088	1.578
0.50	0.457	0.096	1.553
1.00	0.155	0.071	1.227
1.50	0.019	0.088	1.108
2.00	0.0	0.042	1.042
2.50	0.0	0.016	1.016
3.00	0.0	0.010	1.010

FIG. 4. Zero-frequency dielectric function for solid argon.

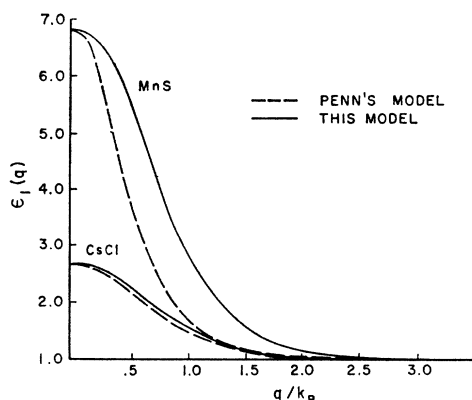[30] J. Callaway, *Energy Band Theory* (Academic Press Inc., New York, 1964).

FIG. 6. Zero-frequency dielectric function for MnS and CsCl.

argon is shown on the same graph, and, although the static limit for this model was adjusted to be slightly different from Hermanson's value, agreement is fair except for large q, where $\epsilon(q)-1$ has a q^{-2} dependence for Hermanson's model and q^{-4} for this model. Penn's[17] interpolation formula for the two-parameter-model semiconductor is also plotted for comparison with the two model insulators, taking values of his parameters suitable for argon. It is seen that his interpolation formula compares quite well with this model insulator in the case of argon.

A question of interest which can be answered by this calculation is the magnitude of umklapp contributions to the dielectric function. Table II shows contributions to $\epsilon(q)$ for argon from normal and umklapp processes separately. The significant result for this model is that for small $q \lesssim k_B$ umklapp terms are almost negligible, while for $q \gtrsim k_B$ they begin to dominate. Since $\epsilon(q)$ falls sharply at k_B, strong screening is dominated by normal processes, which implies that average screened exchanged potentials, such as the ones discussed in Sec. VI, will be affected only slightly by umklapp processes. This result is found generally in all solids studied here and at all frequencies except near a plasma frequency of the p bands.

Dielectric functions for the other solids listed in Table I are shown in Figs. 5, 6, and 7. Figure 5 shows Azuma's[19] calculation for KCl compared to Penn's model and this model. While the two models agree quite well, Azuma's calculation deviates from them both substantially. This discrepancy is likely due to the limited number of terms which he included in his sum in the Brillouin zone: only 14 points. He found that 1500 points were required to give $\epsilon(0)$ correctly, so his 14-term sum, which overestimates $\epsilon(0)$, possibly overestimates $\epsilon(q)$ at other q also. Agreement between Penn's interpolation formula and this model is even closer for KCl than for Ar. The same is true for CsCl, but MnS shows substantial differences between the models for $q < 2k_B$. In the latter two insulators there are presently no other calculations available for comparison.

In the case of silicon it might be presumed that this model would be a poor one, since valence bands are more free-electron-like. The energy bands in this model are parabolic, however, so the principal difference will be in matrix elements of the valence and conduction wave functions. Figure 7 shows $\epsilon(q)$ for silicon. At first E_g was taken as 1 eV, but, since agreement with Nara's[20] calculation for silicon was poor, $\epsilon(q)$ was also obtained for $E_g=4$ eV, which is a reasonable value for the average band gap, in an attempt to make the true band structure better approximated by the present one. In neither case does the result produce Nara's detailed structure, although the latter case does agree better with Penn's result. For large q this model underestimates $\epsilon(q)$, probably because of the method of adjusting $\epsilon(q)$ at $q=0$.

The wave number and frequency dependence of the dielectric function has been obtained for argon and is displayed in Fig. 8. Only a few values of q were used due to the amount of computer time required. For frequencies less than E_g, $\epsilon(\mathbf{q},\omega)$ is almost independent of ω, justifying the common use of static screening in this frequency range. Band transition frequencies are $1 < \omega/E_g < 1.3$ for argon, and it is in this region that $\epsilon_1(\mathbf{q},\omega)$ passes through maximum, zero, and minimum values. At frequencies greater than $2.5E_g$, effects of $3p$ bands diminish, and $\epsilon(\mathbf{q},\omega)=1$. Since the lower-lying bands are even narrower than the $3p$ bands and lie about 2-3 E_g below the $3p$ bands, their effects should not begin until effects of $3p$ bands have died out. The $3p_x$ and $3p_z$ bands are not identical, however, and the detailed structure in the interband transition frequency range may be traced to this difference. Near a zero of $\epsilon_1^z(\mathbf{q},\omega)$, p_x and p_y bands will not give zero, and will dominate the structure. Furthermore, normal and umklapp contributions to $\epsilon_1^z(\mathbf{q},\omega)$ pass through zero at different frequencies, so that umklapp effects may become strong, especially for large q, as shown for $q=1.5k_B$. The oscillations are due to competition between p_x and p_z bands, as well as between normal and umklapp parts. For $q=0.25k_B$ the undamped
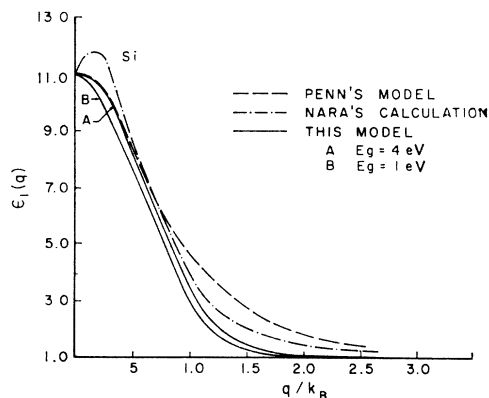

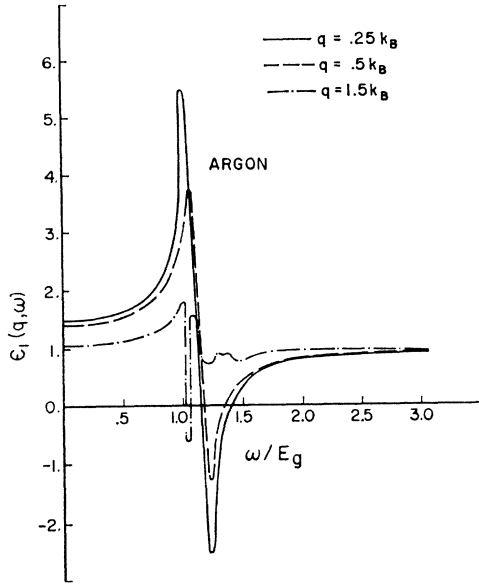FIG. 7. Zero-frequency dielectric function for silicon.

FIG. 8. Real part of the dielectric function for solid argon.

plasma frequency is $1.4E_g = 18.5$ eV, while for $q = 0.5k_B$, $\omega_p = 17.9$ eV. These may be compared to the free-electron value of $\omega_p = (4\pi N e^2/m)^{1/2} = 16.6$ eV.

The imaginary part of $\epsilon(\mathbf{q},\omega)$ is shown in Fig. 9. The dominant features are the two strong peaks which are maxima of the p_x and p_z band contributions, respectively. The zeros of $\epsilon_1(\mathbf{q},\omega)$ which occur there correspond to strongly damped plasmons. Comparing curves for $q = 0.25k_B$ and $q = 0.5k_B$, it is clear that this model containing the three p valence bands and one conduction band do not satisfy the longitudinal sum rule for $q > 0.5k_B$. To do this it would be necessary to include more valence and conduction bands in the model, or to relax the restriction on wave functions that the measured static limit be obtained. The present approach contrasts with Hermanson's approach, which was to eliminate wave functions (matrix elements) by forcing the sum rule to hold for a two-band model. The approach in this calculation has been: Given energy bands and wave functions, find their contribution independent of any remaining ones (the ones needed to complete the sum rule), but otherwise make as few approximations as possible.

VII. SCREENED EXCHANGE POTENTIALS

Since Slater's original proposal[31] of the $\rho^{1/3}$ exchange potential, there have been a number of modifications or alternatives suggested[32] for it. Some of the proposals are intended to improve the exchange approximation, while others attempt to incorporate correlation effects as well. One of the latter effects was made by Robinson

[31] J. C. Slater, Phys. Rev. **81**, 385 (1951).
[32] A recent paper containing most of the references is D. A. Liberman, Phys. Rev. **171**, 1 (1968).

et al.,[33] who screened the Coulomb interaction with the Thomas-Fermi dielectric function before performing the Slater average. The Slater average may be simplified to[33]

$$V_{\text{ex}} = -\frac{2k_F}{\pi^2} \int_0^1 (2k_F x)^2 \mathcal{U}(2k_F x)[1 - \tfrac{3}{2}x + \tfrac{1}{2}x^3]dx, \quad (6.1)$$

where

$$\mathcal{U}(2k_F x) = \mathcal{U}(q) = V(q)/\epsilon(q)$$

is the Fourier transform of the screened interaction. Inserting the Thomas-Fermi dielectric function,

$$\epsilon(q) = 1 + q_{\text{TF}}^2/q^2, \quad (6.2)$$

Robinson obtained

$$V_{\text{RBKS}} = -6[(3/8\pi)\rho]^{1/3}\{1 - \tfrac{4}{3}\alpha \tan^{-1}(2/\alpha)$$
$$+ \tfrac{1}{2}\alpha^2 \ln(1 + 4\alpha^{-2}) - \tfrac{1}{6}\alpha^2[1 - \tfrac{1}{4}\alpha^2 \ln(1 + 4\alpha^{-2})]\}, \quad (6.3)$$

where $\alpha \equiv q_{\text{TF}}/k_F = 0.646\rho^{-1/6}$.

This approach to an exchange potential could be improved in two respects. First, if the exchange potential is to be used in atoms or in insulating or semiconducting solids, a correction to the small q screening should be made. Instead of approaching an appropriate finite $\epsilon(0)$, the Thomas-Fermi function diverges in this limit, indicative of a free gas of electrons instead of bound electrons, and greatly overestimates screening for small q. A second factor related to this is the absence of any treatment of covalency or solid-state effects in the Thomas-Fermi dielectric function.

The dielectric function of the model insulator developed in this paper does not suffer from these deficiencies, but on the other hand, calculations using it in (6.1) would necessitate numerical work, while an analytic expression like (6.3) would be much more convenient. In view of close agreement obtained between this model and Penn's interpolation formula,[17] substitution of the interpolation formula should not cause serious error in a screening calculation.
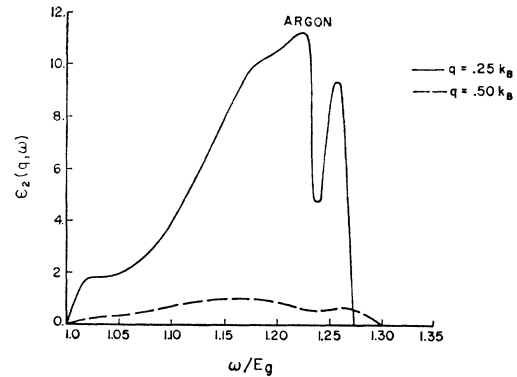

FIG. 9. Imaginary part of the dielectric function for solid argon.

[33] J. E. Robinson, F. Bassani, R. S. Knox, and J. Schrieffer Phys. Rev. Letters **9**, 215 (1962), hereafter referred to as RBKS.

Penn's formula is

$$\epsilon(q) = 1 + (\hbar\omega_p/E_g)^2 F [1 + (E_F/E_g)(q/k_F)^2 F^{1/2}]^{-2}, \quad (6.4)$$

where

$$F \equiv 1 - E_g/4E_F + \tfrac{1}{3}(E_g/4E_F)^2,$$

and ω_p is the usual plasma frequency. Defining

$$A = (\hbar\omega_p/E_g)F^{1/2}, \quad B = 4(E_F/E_g)F^{1/2},$$

the Penn screened exchange potential is

$$V_{\text{Penn}} = -\frac{6}{\pi}k_F \int_0^1 \frac{[1 - \tfrac{3}{2}x + \tfrac{1}{2}x^3]}{[1 + A^2/(1+Bx^2)^2]}dx. \quad (6.5)$$

The integral is not simple, but can be worked out exactly to give

$$V_{\text{Penn}} = -6\left[\frac{3}{8\pi}\rho\right]^{1/3}\left[1 + \frac{4}{3}\left[\frac{A}{2B}\left(3 + \frac{1}{B}\right)\left(\tan^{-1}\frac{B+1}{A} - \tan^{-1}\frac{1}{A}\right) - \frac{A^2}{4B^2}\ln\frac{B(B+2)+(1+A^2)}{(1+A^2)}\right]\right.$$

$$-\frac{4}{3}\frac{A}{[2B(1+A^2)]^{1/2}}\left\{[(A^2+1)^{1/2}-1]^{1/2}\tan^{-1}\frac{[2B((A^2+1)^{1/2}-1)]^{1/2}}{(A^2+1)^{1/2}-B}\right.$$

$$\left.\left. + \tfrac{1}{2}[(A^2+1)^{1/2}+1]^{1/2}\ln\left[\frac{(A^2+1)^{1/2}+B+[2B((A^2+1)^{1/2}-1)]^{1/2}}{(A^2+1)^{1/2}+B-[2B((A^2+1)^{1/2}-1)]^{1/2}}\right]\right\}\right]. \quad (6.6)$$

It should be noted that all the covalent and solid-state effects of this calculation are brought into this screened exchange potential explicitly with one additional parameter E_g, although these effects enter implicitly through the procedure used to obtain the interpolation formula.

One remaining question is the application of (6.6) to a specific solid. Slater's exchange potential or (6.3) can be made local in the usual way by letting n be a function of r. In the case of (6.6) there are two adjustable parameters to deal with: n and E_g. The former could be treated as before, while the latter parameter could be determined from experimental observations of the minimum or average gap characterizing the solid. However, the important point for the screening calcula-

FIG. 10. Screened exchange potentials for the chlorine ion in CsCl.

tion is that $\epsilon(0)$ be reasonable. Since $\epsilon(0)$ is determined in Penn's model by both $n(r)$ and E_g, as n varies, $\epsilon(0)$ will also vary, with the result that at some finite densities there turns out to be no screening at all. This unphysical result can be avoided if n and E_g are both taken as functions of r, $E_g(r)$ being determined by the condition that the correct $\epsilon(0)$ always be obtained for a given $n(r)$. This approximation, which is analogous to Phillips's treatment of n and E_g on an equivalent basis, might be described as a local semi-conducting electron-gas approximation.

A comparison of Slater's exchange, the RBKS exchange, and exchange calculated with Penn's formula is shown in Fig. 10, as calculated for parameters appropriate to the chlorine ion in a cesium chloride crystal. The effect of screening is evidently strong; Thomas-Fermi screening, as expected, produces the greatest reduction in the exchange potential. Both screening methods reduce the Slater exchange potential everywhere, but especially important is the reduction in the tail of the chlorine exchange potential. While Penn's dielectric screening is more moderate at intermediate distances from the chlorine nucleus, choice of one of these local exchange potentials over another must await numerical calculations in a full band calculation. Whether a clear choice can be made even then is not certain.
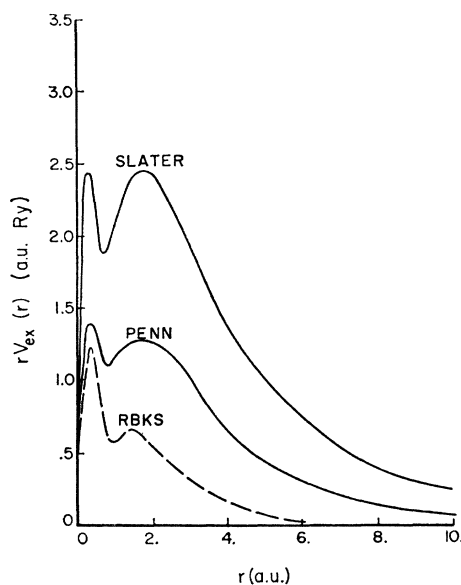
VIII. CONCLUSIONS

The model insulator proposed in this paper has proved capable of yielding the static dielectric constant of real insulators when band parameters are properly chosen. Results for the dielectric function at finite q and ω appear to be reasonable and, at zero frequency, are in essential agreement with the interpolation formula proposed by Penn to fit his numerical results for semi-conductors. In evaluating the dielectric function for

the model insulator it was found that for $q > k_B$ umklapp contributions, as defined here, were more important than normal, while for $q \leq k_B$ the reverse is true.

Dielectric screening using this model produced screened exchange potentials which were intermediate to the completely screened results of RBKS and the completely unscreened exchange potential of Slater. However, it is very difficult to select one exchange potential over another, since this choice may be decided only after a complete band-structure calculation.

The model could be improved in several respects, especially by including higher conduction bands. In this way the longitudinal sum rule could be satisfied. At present the limited knowledge of conduction bands in insulators does not warrant the added complexity in this simple model, although free-electron bands could probably serve as a simple approximation to the higher bands for this purpose in many cases.

ACKNOWLEDGMENTS

APPENDIX

The integrals needed for evaluating matrix elements with the wave functions U_0 and U_1 defined by Eqs. (3.15) and (3.16) may be worked out exactly to give

$$\int_0^\infty j_0(kr) U_0(r) r^2 dr = \left[\tfrac{1}{2}(2\gamma)^3 \right]^{1/2} \frac{2\gamma}{(\gamma^2 + k^2)^2},$$

$$\int_0^\infty j_0(qr) U_0(r) U_1(r) r^2 dr$$

$$= \left[\frac{(2\gamma)^3}{2} \frac{(2\delta)^5}{24} \right]^{1/2} \frac{2[3(\gamma+\delta)^2 - q^2]}{[(\gamma+\delta)^2 + q^2]^3},$$

$$\int_0^\infty j_0(qr) |U_1(r)|^2 r^2 dr = \frac{(2\delta)^6 [(2\delta)^2 - q^2]}{[(2\delta)^2 + q^2]^4},$$

$$\int_0^\infty j_1(kr) U_1(r) r^2 dr = \left[\frac{(2\delta)^5}{24} \right]^{1/2} \frac{8\delta k}{(\delta^2 + k^2)^3},$$

$$\int_0^\infty j_2(qr) |U_1(r)|^2 r^2 dr = \frac{2(2\delta)^6 q^2}{[(2\delta)^2 + q^2]^4}.$$